Streamflows over a West African Basin from the ALMIP2 Model Ensemble

Augusto Getirana, Aaron Boone, Christophe Peugeot, S. Ait-Mesbah, J. Polcher, M. Anderson, G. Balsamo, S. Boussetta, E. Dutra, F. Pappenberger, et al.

Streamflows over a West African Basin from the ALMIP2 Model Ensemble

AUGUSTO GETIRANA

NASA Goddard Space Flight Center, Greenbelt, and Earth System Science Interdisciplinary Center, University of Maryland, College Park, College Park, Maryland

AARON BOONE

CNRM-GAME/Météo-France, Toulouse, France

CHRISTOPHE PEUGEOT

HydroSciences Montpellier, Montpellier, France

ALMIP2 WORKING GROUP[a]

(Manuscript received 26 September 2016, in final form 9 December 2016)

ABSTRACT

Comparing streamflow simulations against observations has become a straightforward way to evaluate a land surface model's (LSM) ability in simulating water budget within a catchment. Using a mesoscale river routing scheme (RRS), this study evaluates simulated streamflows over the upper Ouémé River basin resulting from 14 LSMs within the framework of phase 2 of the African Monsoon Multidisciplinary Analysis (AMMA) Land Surface Model Intercomparison Project (ALMIP2). The ALMIP2 RRS (ARTS) has been used to route LSM outputs. ARTS is based on the nonlinear Muskingum–Cunge method and a simple deep water infiltration formulation representing water-table recharge as previously observed in that region. Simulations are performed for the 2005–08 period during which ground observations are largely available. Experiments are designed using different ground-based rainfall datasets derived from two interpolation methods: the Thiessen technique and a combined kriging–Lagrangian methodology. LSM-based total runoff (TR) averages vary from 0.07 to 1.97 mm day^{-1}, while optimal TR was estimated as ~0.65 mm day^{-1}. This highly affected the RRS parameterization and streamflow simulations. Optimal Nash–Sutcliffe coefficients for LSM-averaged streamflows varied from 0.66 to 0.92, depending on the gauge station. However, individual LSM performances show a wider range. A more detailed rainfall distribution provided by the kriging–Lagrangian methodology resulted in overall better streamflow simulations. The early runoff generation related to reduced infiltration rates during early rainfall events features as one of the main reasons for poor LSM performances.

1. Introduction

One of the goals of the African Monsoon Multidisciplinary Analysis (AMMA) Land Surface Model Intercomparison Project (ALMIP; Boone et al. 2009b) is to better understand key processes and their corresponding scales over West Africa through state-of-the-art land surface models (LSMs) forced with high-quality observational datasets. Phase 2 of ALMIP (ALMIP2; Boone et al. 2009a; www.cnrm.meteo.fr/amma-moana/amma_surf/almip/index.html) focuses on the model evaluation at local and mesoscales over Mali, Niger, and Benin. As part of ALMIP2, this study focuses on the Benin mesoscale region, more specifically, the upper Ouémé River basin, located in the northern part of the country. The basin drains an area of about 14 400 km^2 (see Fig. 1) and is characterized by the Sudanian climatic regime with a single rainy season averaging 1200 mm yr^{-1}. More details about the region's hydrology can be found in the literature (e.g., Varado et al. 2006; Giertz et al. 2006; Le Lay et al. 2008; Gaiser et al. 2008; Peugeot et al. 2011; Getirana et al. 2014a).

[a] Please see the appendix for the full list of working group members.

Corresponding author e-mail: Augusto Getirana, augusto.getirana@nasa.gov

DOI: 10.1175/JHM-D-16-0233.1

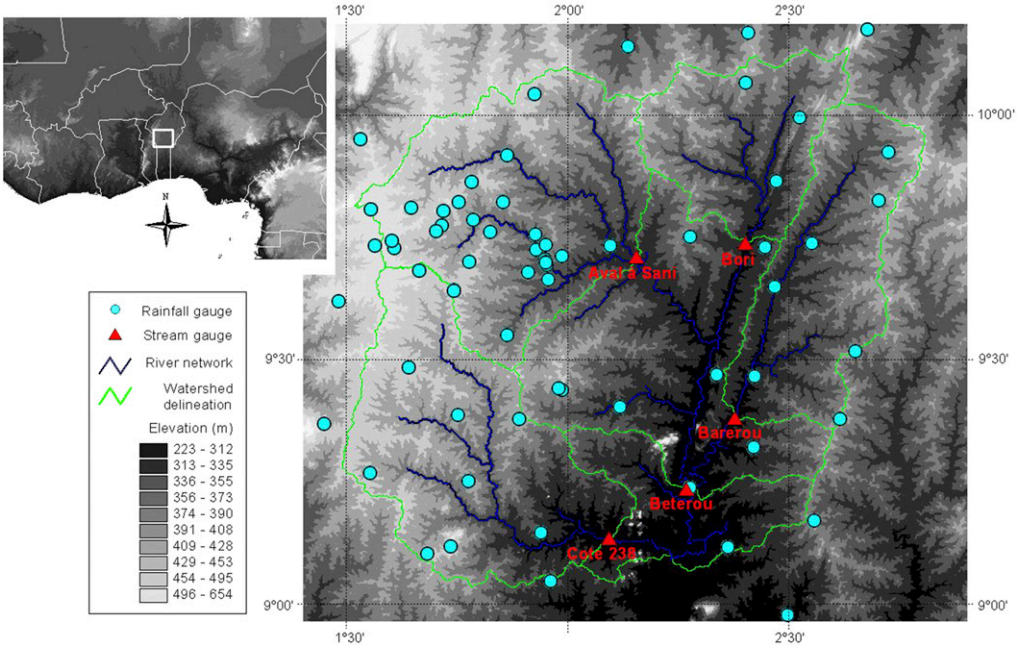

FIG. 1. Geographical location of the upper Ouémé River basin.

The objectives of this study are to evaluate the ability of 14 LSMs to simulate the mesoscale hydrology in the selected area, given their variable representation of such processes; to investigate possible structural biases in LSMs that result from the inadequate or missing representation of key processes; and to assess impacts of two different precipitation datasets on LSM-based water budget simulations. These objectives are well aligned with previous multimodel intercomparison initiatives (van den Hurk et al. 2011), such as such as the Project for the Intercomparison of Land-Surface Parameterization Schemes (PILPS) and its different phases (e.g., Henderson-Sellers et al. 1995; van den Hurk and Viterbo 2003; Wood et al. 1998), the Global Soil Wetness Project phase 1 (GSWP-1; Dirmeyer et al. 1999) and phase 2 (GSWP-2; Dirmeyer et al. 2006), the Rhône-Aggregation Land Surface Scheme intercomparison project (Boone et al. 2004), and phase 1 of ALMIP (ALMIP1; Boone et al. 2009b).

Precipitation fields are evaluated by performing two experiments for each LSM forced with databases derived from different interpolation procedures. The evaluation is performed by comparing simulated and observed river streamflows at gauging stations located within the basin. This method has been considered in previous studies as a straightforward way to evaluate 1) the water budget provided by LSMs at different spatial and temporal scales (e.g., Lohmann et al. 1998; Boone et al. 2004; Getirana et al. 2014b) and 2) precipitation datasets (Yilmaz et al. 2005; Getirana et al. 2011; Li et al. 2015; Zubieta et al. 2015). Its main advantage is the fact that streamflow can be directly measured, with cost-effective methods, at almost any location. Additionally, water discharge gives a spatially distributed measure of model performance, with the one caveat that compensating errors can occur.

The ALMIP2 River Routing Scheme (ARTS; Getirana et al. 2014a) is utilized in this study to simulate the river flow dynamics in the upper Ouémé River basin in an effort to identify inadequate or missing representation of key processes in LSMs that could result in possible structural biases. ARTS's river flow directions and geometry are derived from multiple data sources, including in situ observations and/or satellite imagery. Four parameters (the Manning's river flow roughness coefficient and three others related to the representation of time delays and aquifers) are particularly sensitive to the representation of physical processes in LSMs, requiring either expertise or calibration in order to be determined (Getirana et al. 2014a). In this sense, an automatic calibration approach is adopted in order to obtain optimal parameter sets and streamflow simulations from modeling experiments.

2. Datasets

a. *Meteorological forcing and surface parameters*

Two precipitation products were derived from the AMMA–Coupling the Tropical Atmosphere and the Hydrological Cycle (AMMA-CATCH) observing system (Lebel et al. 2009) using different interpolation

TABLE 1. Selected streamflow gauges located within the upper Ouémé River basin.

Station	Lat	Lon	Area (km^2)	Observed discharge (m^3 s^{-1})	Observed runoff rate (mm day^{-1})	Rainfall (mm day^{-1})	Runoff/rainfall ratio
Beterou	9.20°N	2.27°E	10 140	43.13	0.37	3.01	0.12
Aval-Sani	9.72°N	2.15°E	3307	17.54	0.46	2.99	0.15
Bori	9.76°N	2.40°E	1630	4.86	0.26	2.98	0.09
Barerou	9.36°N	2.38°E	2141	8.03	0.32	3.07	0.10
Cote 238	9.09°N	2.09°E	3152	17.61	0.48	3.13	0.15

techniques: 1) the nearest neighbor [or Thiessen interpolation method (THI)] and 2) a combined kriging–Lagrangian methodology (LAG; Vischel et al. 2009). This method has been developed in order to capture the main features of organized convective activity, such as squall lines, which condition the spatial rainfall distribution. When convection is not organized, then the default kriging method is used. The resulting products are available for the 2005–08 period at a 30-min time step and 0.05° spatial resolution.

Mesoscale downwelling longwave and shortwave radiative fluxes (also at a 0.05° spatial resolution and aggregated from a 15- to a 30-min time step for this project) are from the Land Surface Analysis Satellite Applications Facility (LSA SAF; Geiger et al. 2008; Trigo et al. 2011). These fluxes are interpolated from their native 3-km grid to the 0.05° grid (approximately 6 km at the latitudes used in this study) used in ALMIP2. The European Centre for Medium-Range Weather Forecasts (ECMWF) operational forecast system is the source of other meteorological forcings (Boone et al. 2009a). Relatively small hypsometric-based adjustments using the differences between the large-scale model and ALMIP2 mesoscale topography were applied to the temperature, specific humidity, and surface pressure. Albedo and the leaf area index (LAI) are from the ECOCLIMAP2 database (Kaptué Tchuenté et al. 2011), including interannual vegetation variability, which is highly significant over the region.

b. Streamflow

Streamflow observations at five gauging stations draining main catchments within the basin (Beterou, Aval-Sani, Bori, Barerou, and Cote 238) were used in the modeling experiments described below. These stations are operated by AMMA-CATCH and their locations are shown in Fig. 1. Their drainage areas vary from 1630 km^2 (Bori station) to 10 140 km^2 (Beterou station), with mean streamflows ranging from 4.86 to 43.1 m^3 s^{-1}. These stations were selected because they drain the main tributaries of the upper Ouémé River. It is worth noting that all gauging stations, except for Cote 238, are related to an interconnected river network draining to Beterou. The branch draining to Cote 238 connects to the main stem farther downstream. The main characteristics of the catchments are listed in Table 1.

3. LSM intercomparison approach

a. The ALMIP2 land surface models

As mentioned before, 14 ALMIP2 LSMs are evaluated in this study. They are the Canadian Land Surface Scheme (CLASS; Verseghy 1991); CLM (Lawrence et al. 2011); Catchment LSM (CLSM; Ducharne et al. 2000); CLSM-NASA (Koster et al. 2000); HTESSEL (Balsamo et al. 2011); ISBA (Noilhan and Mahfouf 1996); JULES (Clark et al. 2011); MOSAIC (Koster and Suarez 1992); Noah (Decharme et al. 2009); Minimal Advanced Treatments of Surface Interaction and Runoff (MATSIRO; Takata et al. 2003); ORCHIDEE (Krinner et al. 2005); Suivi de l'Etat Hydrique des Sols (SETHYS; Coudert et al. 2008); Simple Biosphere Model including Urban Canopy (SiBUC; Tanaka and Ikebuchi 1994); and Soil, Water, Atmosphere, and Plant (SWAP; Gusev and Nasonova 1998). Water budget simulations are evaluated in terms of streamflows derived from ARTS. LSMs and ARTS were coupled in offline mode (i.e., no feedbacks from ARTS to the LSMs are considered). This section provides a brief description of ARTS and the LSM intercomparison design.

b. ARTS

ARTS was developed within the framework of ALMIP2 with the objective of evaluating the water budget simulated by LSMs. A full description of the model can be found in Getirana et al. (2014a), and only the main features are briefly provided below. ARTS is forced by surface runoff R and base flow B derived from LSMs. Variables R and B go through two linear reservoirs before reaching the river network in order to represent their time delays (e.g., Getirana et al. 2012). The surface runoff time delay τ_r (day) is the product of a spatially distributed surface runoff time delay factor $T_r(\Delta t)$, determined by the Kirpich (1940) formula, and a

spatially uniform parameter p_r (unitless). The baseflow time delay τ_b (day) is also spatially uniform. The model also simulates the deep water infiltration (DWI) using a simple formulation. At each time step, a spatially uniform fraction f of B, called subsurface flow B' ($B' = Bf$), is transferred to the river network while the remaining part, referred to as deep water infiltration [DWI = $B(1 - f)$], leaves the system to an assumed deep aquifer, which is not specifically diagnosed by most LSMs. Considering water losses and water-table recharge are essential over the Ouémé River basin, since previous studies based on observed data (Kamagaté et al. 2007; Séguis et al. 2011) estimated recharge rates ranging from 10% to 17% of the annual rainfall depending on the year. For simplification, all of the model parameters are constant in time.

Surface runoff and baseflow linear reservoir outputs are then routed through the river network using the nonlinear Muskingum–Cunge (MC) method (Cunge 1969; Ponce 1989). The model simulates spatially distributed streamflow at a daily time step. Its internal computational time steps can be adjusted to improve numerical accuracy, as a function of river geometry and flow dynamics. In this study, the ARTS internal computational time step was set as 1 h, and the spatial resolution is 0.05° × 0.05°. ARTS parameters such as river length and slope, flow direction, and drainage area were derived from the Shuttle Radar Topography Mission (SRTM; Farr et al. 2007) digital elevation model (DEM) data. River widths were determined as a function of the drainage area based on a power-law relation using cross-sectional observations at 12 gauges.

c. Experimental design

As in Getirana et al. (2014a), for each experiment, ARTS parameters were automatically calibrated for the period from 2005 to 2008 using the Multiobjective Complex Evolution of the University of Arizona (MOCOM-UA) global multiobjective optimization algorithm (Yapo et al. 1997, 1998; Boyle et al. 2000). MOCOM-UA allows the optimization of multiple objective functions (OFs), providing a distribution of solutions in the Pareto optimum space (Pareto 1971), only requiring the definition of the population of points n_s randomly distributed within the parameter hyperspace. Previous studies have calibrated river routing scheme parameters forced by multiple LSM outputs (e.g., David et al. 2013). Getirana et al. (2014a) compared three optimization approaches: 1) one using observations at a Beterou station; 2) another using data at five gauging stations (listed in Table 1), but individual calibrations were performed for their respective catchments; and 3) a third one using five gauging stations simultaneously. The authors concluded that the third approach is cost efficient and still provides good overall results. In this sense, that approach was adopted in this study.

The Nash–Sutcliffe (NS) coefficient and the normalized root-mean-square error (NRMSE) for streamflow are considered in the optimization process:

$$\mathrm{NS} = 1 - \frac{\sum_{t=1}^{n_t} (y_t - x_t)^2}{\sum_{t=1}^{n_t} (y_t - \overline{y}_t)^2} \quad \text{and} \tag{1}$$

$$\mathrm{NRMSE} = \frac{\mathrm{RMSE}}{(y_{\max} - y_{\min})}, \tag{2}$$

where t is the time step and n_t represents the total number of days with observed data. The variables x_t and y_t are the simulated and target (observed) signals at time step t, respectively, while $y_{\max}$, $y_{\min}$, and $\overline{y}$ represent the respective maximum, minimum, and mean values of the target signals for the entire period. The NS coefficient ranges from $-\infty$ to 1, where 1 is the optimal case, while 0 results when simulations represent observed signals as well as the mean value. The NRMSE varies from 0 to $+\infty$, where 0 is the optimal value.

Objective functions are a result of weighted sums of each coefficient at gauge station, as defined below (Getirana et al. 2013):

$$\mathrm{OF}_1 = \text{maximize}\left[\sum_{k=1}^{n} \mathrm{NS}_k(W_k)\right] \quad \text{and} \tag{3}$$

$$\mathrm{OF}_2 = \text{minimize}\left[\sum_{k=1}^{n} \mathrm{NRMSE}_k(W_k)\right], \tag{4}$$

where n stands for the total number of gauge stations and W is the weight attributed to each of them, defined as

$$W_k = \frac{A_k}{\sum_{k=1}^{n} (A_k)}, \tag{5}$$

where A represents the drainage area of gauge station k.

Two runs were performed for each LSM using 1) THI and 2) LAG, totaling 28 realizations. The parameters τ_b, p_r, and f were automatically calibrated in the optimization runs. First guesses and parameter domains used in the automatic calibration are the same as suggested in Getirana et al. (2014a). The value of n_s was fixed as 200. Results were evaluated using two additional coefficients: the delay index (DI; days) and the streamflow relative error (RE; unitless). The DI is used to measure errors related to the time delay between the simulated

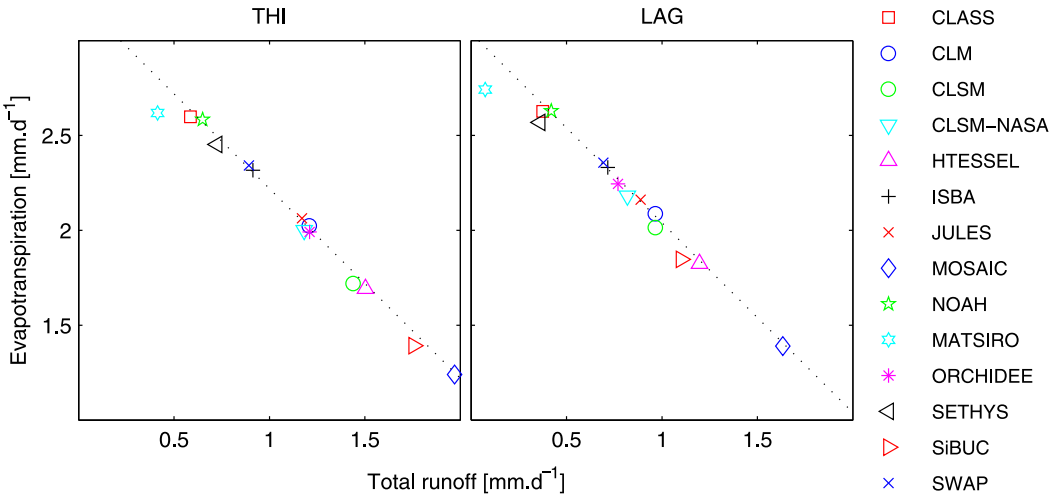

FIG. 2. Average precipitation repartition in evapotranspiration and total runoff (sum of surface runoff and base flow) over the upper Ouémé River basin for the 2005–08 period. Dotted lines indicate where points should be positioned if $P = \mathrm{ET} + \mathrm{TR}$.

and the observed hydrographs. The coefficient is computed using the cross-correlation function $R_{xy} = f(m)$ from simulated x and observed y time series, where DI equals the value of the time lag m when R_{xy} is maximum. The RE is defined as

$$\mathrm{RE} = \frac{\sum_{t=1}^{n_t} x_t - \sum_{t=1}^{n_t} y_t}{\sum_{t=1}^{n_t} y_t}; \tag{6}$$

RE allows us to determine whether mean simulations under/overestimate observations. For positive variables, such as streamflows, RE values vary from -1 to $+\infty$, where 0 is the optimal value.

4. Results and discussion

a. LSM ensemble water budget

The simulated total runoff (TR; defined as the sum of the surface runoff and baseflow components, i.e., $R + B$) and evapotranspiration (ET) are evaluated in order to determine the impacts of precipitation datasets on the water budget, and how LSMs represent the long-term precipitation repartition at the basin scale. Figure 2 shows mean TR and ET rates simulated in each modeling experiment using THI and LAG. Mean precipitation rates slightly differ between the two products: THI, with 3.22 mm day^{-1}, exceeds the LAG (3.04 mm day^{-1}) by 6%. This relatively small average difference results in major changes in R, B, and ET. Based on the multimodel mean and standard deviation, one can determine that the increased P rate from THI is followed by an overall increase of TR (0.34 ± 0.13 mm day^{-1}, or 44% ± 17%) and decrease of ET (−0.14 ± 0.13 mm day^{-1}, or −6% ± 6%), when compared against LAG results. The percentage is computed as a function of the multimodel mean derived from LAG experiments. ISBA and SWAP have minor changes in ET (−0.01 mm day^{-1}), converting most of the increased P into TR (0.20 mm day^{-1}). SiBUC, CLSM, and ORCHIDEE had TR significantly impacted, with increases of 0.66, 0.48, and 0.44 mm day^{-1}, respectively.

ET/TR ratios vary from a model to another, and extreme results are obtained using MATSIRO-LAG, with TR = 0.07 mm day^{-1} (or 0.02P) and ET = 2.74 mm day^{-1} (or 0.90P), and MOSAIC-THI, with TR = 1.97 mm day^{-1} (or 0.61P) and ET = 1.24 mm day^{-1} (or 0.38P). MOSAIC is the only model resulting in TR > ET in both experiments, and SiBUC presents this characteristic in the THI experiment. A nonnegligible soil moisture increase during the experiment period is noticed in MATSIRO outputs, resulting in TR + ET < P. This can be attributed to either not long enough spinups or the few number of years of simulation where models may not keep a neutral water storage change.

The monthly climatology of R, B, and ET varies significantly from a model to another, as shown in Figs. 3 and 4 for the LAG experiment. Average R and B rates for LAG are 0.50 and 0.28 mm day^{-1}, respectively, and both have peaks in September. However, some models fail in consistently representing the temporal variability of these variables. For instance, either R or B rates are negligible or nonexistent in realizations using CLASS, CLSM-NASA, and MATSIRO. This is explained by the fact that CLASS and MATSIRO do not have subgrid

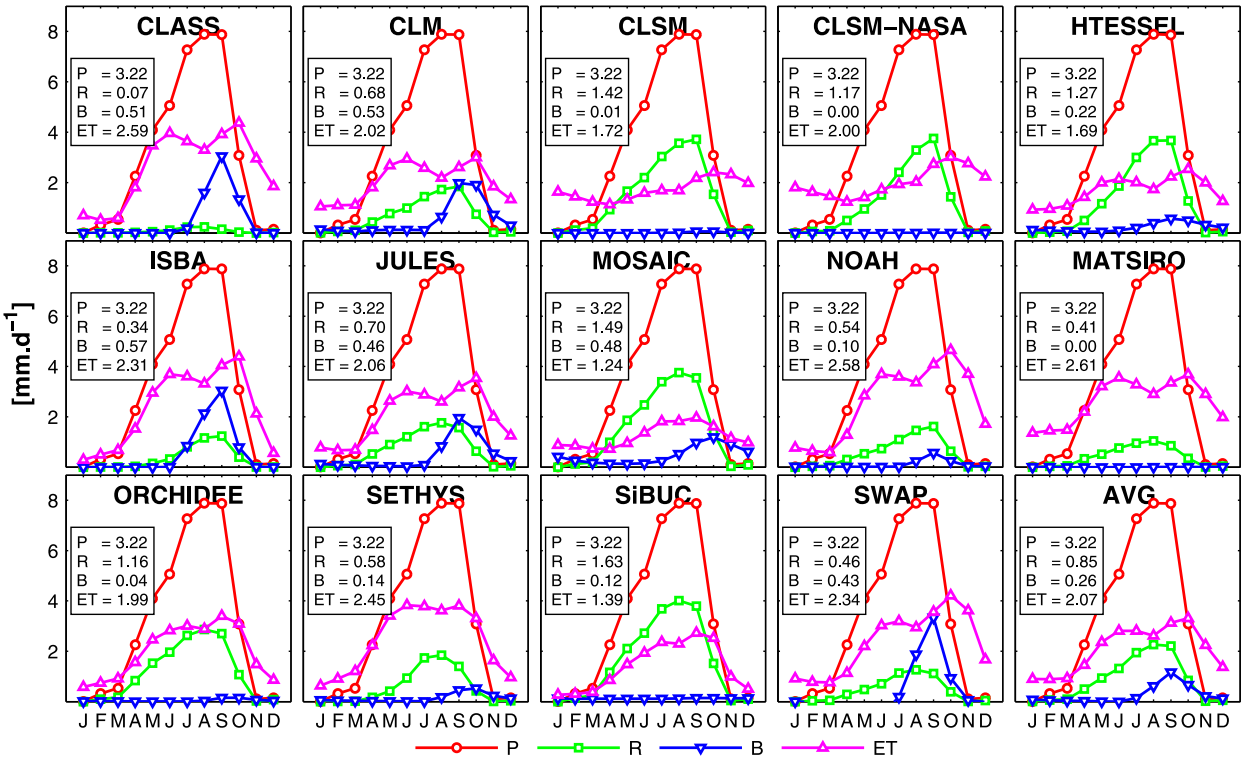

FIG. 3. Water budget variables over the upper Ouémé River basin derived from THI-based precipitation experiments: *P*, *R*, *B*, and ET. Values are monthly averages for the 2005–08 period.

surface runoff parameterizations. In the case of CLSM-NASA, the opposite happens. That LSM has a very strong surface runoff parameterization, thereby removing a lot of water and thus leaving little for *B* and *E*.

Monthly ET rates are generally low from January to March. Other dry months (October–December) preceded by the wet season present a decreasing, but still high, ET rate due to the water storage in the soil during those months. Values can be $1\,\mathrm{mm\,day^{-1}}$ or lower during that period, depending on the LSM.

According to Fig. 5, the potential ET (or PE) reaches minimal values in August, during the monsoon period, and maximal values in March, during the dry season. This pattern reflects the reduced incoming solar radiation due to the cloud cover in the core of the monsoon season. PE in the region is opposite to the LAI signal, also shown in Fig. 5, reaching its maximal values in August. This reflects the phenology of the vegetation, that is, very little green vegetation remains in the dry season (grass cover dries out and trees, mainly from deciduous species, have lost their leaves), and grass cover growth and tree leaf renewal rapidly starts with the first rain events. Model results are consistent with the aforementioned patterns. ET is limited by both soil evaporation (few rainfall and low soil moisture availability) and transpiration (low LAI) during the dry season, despite the energy availability, as indicated by PE. ET increases up to PE values when water becomes available in the first soil layers, as a consequence of higher rainfall rates. That explains the double-peaked ET monthly climatology simulated by most LSMs (see Figs. 3, 4) occurring in June and then in October. Exceptions of the aforementioned pattern are CLSM, CLSM-NASA, and MOSAIC, providing minimum ET rates in April and a single peak in September–October. The double-peaked ET produced by these models is consistent with the ground flux observations (eddy covariance) available in the same area (Mamadou et al. 2014).

Differences in precipitation fields observed in THI mainly impact the water repartition among *R*, *B*, and ET, with a nominal impact on their seasonality (Fig. 4). CLSM-NASA and MATSIRO, both with no *B* generation, had *R* significantly decreased and ET increased. Indeed, on average, surface runoff decreased about 40% and evapotranspiration increased 6%. A minor change was perceived in the base flow.

b. ARTS outputs

Each optimization run resulted in 200 solutions, and the best one, that is, the first one in the rank, was

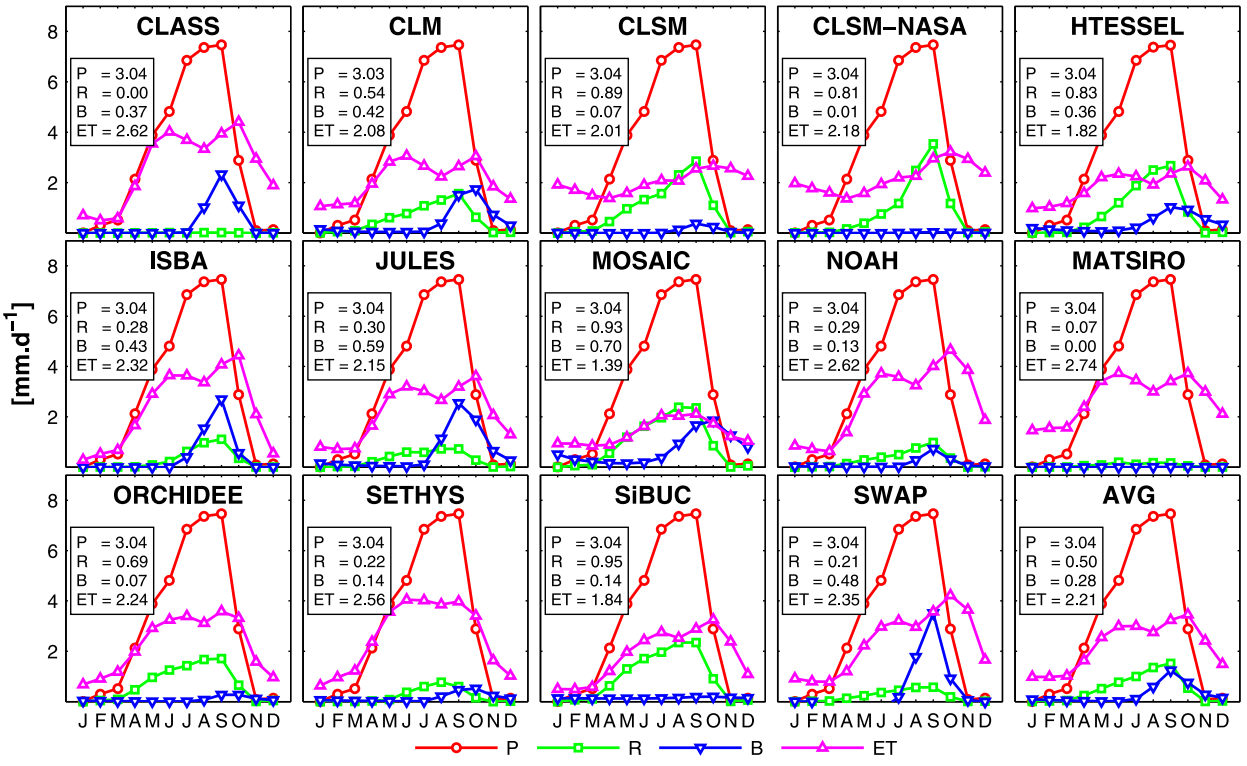

FIG. 4. As in Fig. 3, but for LAG-based precipitation experiments.

selected for evaluation. As shown in Fig. 6, LAG experiments have overall better performances in terms of streamflow simulations, indicating its improved representation of precipitation fields. LAG is particularly better when used in conjunction with six LSMs (CLSM, CLSM-NASA, HTESSEL, MOSAIC, ORCHIDEE, and SiBUC), with an average improvement of NS and NRMSE values (used as OFs in the optimization runs) of 0.54 and 0.05, respectively. Four LSMs (CLM, ISBA, JULES, and SWAP) show negligible changes, and four others (CLASS, Noah, MATSIRO, and SETHYS) had coefficient values that worsened when LAG was used as a forcing, with average deterioration of 0.24 and 0.03, respectively. ISBA-LAG has the best OFs for both experiments, followed by SWAP-LAG. NS and NRMSE coefficients are 0.88 and 0.06 for ISBA and 0.86 and 0.06 for SWAP. Both LSMs present similar hydrological variable climatologies, explaining their similar performances. Poor results were obtained with MOSAIC-THI, SiBUC-THI, and MATSIRO-LAG with negative NS values and NRMSE as high as 0.20.

MOSAIC performed significantly better with LAG (NS = 0.52 and NRMSE = 0.11) than with THI (NS = −0.17 and NRMSE = 0.18), as a result of its sensitivity to changes in precipitation fields, affecting R and B. A 46% higher base flow and 38% lower surface runoff allowed the automatic calibration to increase the amount of DWI and to reduce the water flowing in the river network in MOSAIC-LAG, resulting in better-fitted streamflows. A significant decrease of R is also responsible for improved results in SiBUC-LAG (NS = 0.47 and NRMSE = 0.12), but in this case, B remained basically the same.

Except for the Aval-Sani station, LAG experiments provide overall better results at all gauging stations. ISBA and SWAP feature as the best NS and NRMSE at

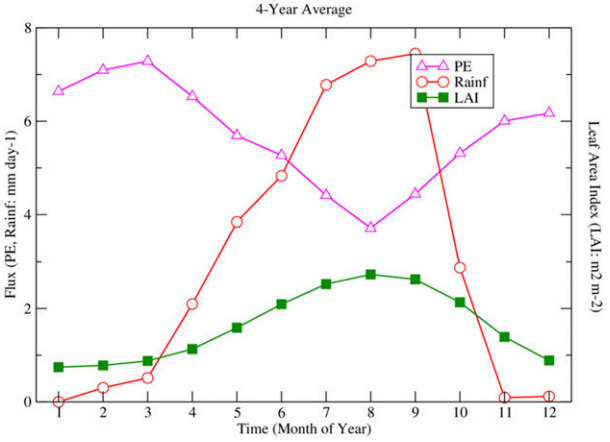

FIG. 5. Monthly mean potential ET vs rainfall vs LAI averaged for the upper Ouémé River basin.

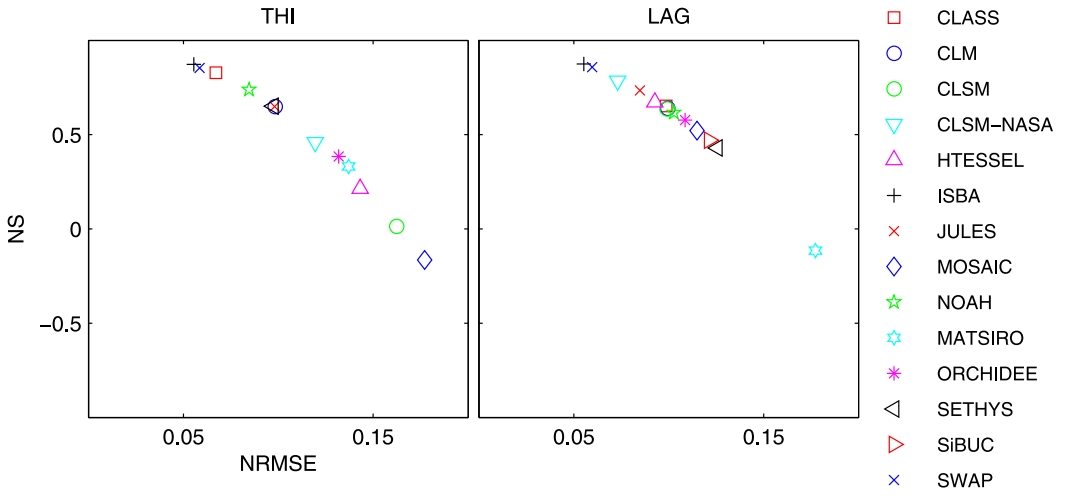

FIG. 6. Best objective functions resulting from optimization runs for experiments using THI- and LAG-based precipitation products.

all stations for both experiments (see Fig. 7). Variable performances at stations expose the impacts of the rainfall monitoring on the accuracy of streamflow simulations. The heterogeneous distribution of coefficients shown in Fig. 7 provides evidence that the kriging–Lagrangian interpolation method results in an overall better rainfall spatial distribution over the basin and, as a consequence, LSMs combined with ARTS are capable of better simulating the water budget and streamflows.

1) PARAMETER SETS

Optimal ARTS parameter sets present a wide range of values. As summarized in Table 2, the average τ_b value for THI experiments is generally higher (22.6 ± 30.2 days) than for LAG experiments (13.5 ± 20.4 days). Average p_r and f values have also been affected, evident by the substantial effect of rainfall accuracy on DWI, and surface runoff and baseflow time delay. Average p_r and f values were nominally affected by rainfall. The high standard deviations observed in all parameters reveal a heterogeneous behavior due to variable water budgets computed by LSMs. For instance, τ_b ranges from 0.1 day (CLASS-LAG) to 91.1 days (HTESSEL-THI), p_r from 37.5 to 250, and f from 0 to 1. The low τ_b value obtained for CLASS-LAG is probably due to the optimization scheme trying to compensate the lack of a

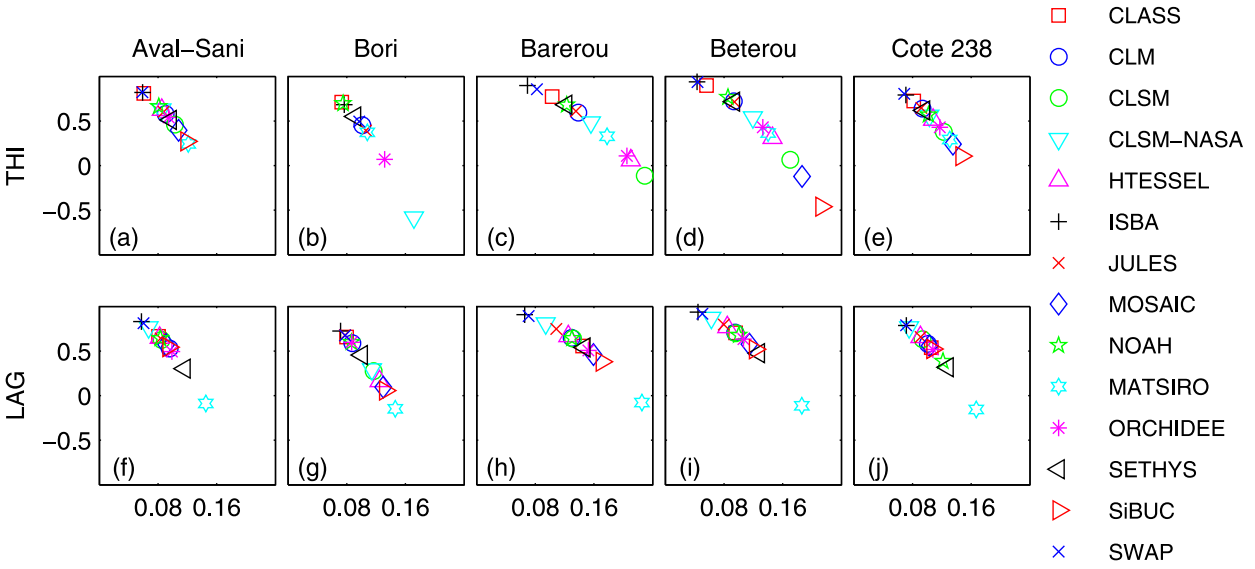

FIG. 7. Best NS (abscissa) and NRMSE (ordinate) coefficients at five stations used to compute the objective functions for experiments using THI- and LAG-based precipitation products.

TABLE 2. Best τ_b (day), p_r (unitless), and f (unitless) derived from the optimization runs.

LSM	THI			LAG		
	τ_b	p_r	f	τ_b	p_r	f
CLASS	0.8	146.8	0.89	0.1	38.4	1.00
CLM	0.3	147.2	0.31	0.3	84.9	0.46
CLSM	55.0	249.9	0.00	39.6	209.7	0.00
CLSM-NASA	24.7	250.0	0.01	63.1	132.0	0.00
HTESSEL	91.1	249.9	0.00	2.4	249.7	0.03
ISBA	9.4	61.5	0.58	5.9	47.0	0.71
JULES	0.5	248.4	0.50	0.5	94.1	0.75
MOSAIC	56.9	249.6	0.00	26.0	249.9	0.00
Noah	0.3	124.7	1.00	0.6	74.7	1.00
MATSIRO	0.9	248.4	0.99	0.7	245.8	0.98
ORCHIDEE	0.1	249.4	0.33	0.4	243.9	0.99
SETHYS	1.0	245.2	1.00	0.6	233.3	1.00
SiBUC	67.8	250.0	0.00	45.9	249.9	0.00
SWAP	7.2	68.2	0.58	3.4	37.5	0.71

fast flow (owing to $R = 0$), minimizing the baseflow time delay.

Generally speaking, timing and magnitude of R and B are the major factors impacting parameters. Overall, high B values result in low f values, as an attempt of the optimization algorithm to match simulated and observed streamflow magnitudes. Exceptions occur when R is too low and B becomes the main source of water to the river network. Experiments using Noah, MATSIRO, and SETHYS obtained f values equal to ~1. This is due to the very low TR generated by these LSMs.

Based on the optimization outputs, one can note in Fig. 8 that TR values should be around 0.65 mm day^{-1} for optimal matching between mean simulated and observed streamflows, that is, RE = 0. As one can see in the figure, most LSMs located on the left side of the plot (except for the two rightmost points representing ISBA and SWAP) produce insufficient TR. This means that the total amount of TR flows to the river network, and no water is left for deep infiltration. On the other hand, LSMs located on the right side of the plot overestimate TR, inducing an increased DWI. Most of these models lose base flow almost entirely as an attempt to match the optimal TR flowing to the river network. These LSMs usually generate high surface runoff rates.

Three LSMs (CLM, CLSM, and CLSM-NASA) have active groundwater schemes. This means that the base flow generated by these models actually corresponds to the subsurface flow. No specific treatment has been made in ARTS for these runs, regarding the existence of a groundwater scheme, and one expects $f = 1$ for these LSMs. However, optimized f values reported in Table 2

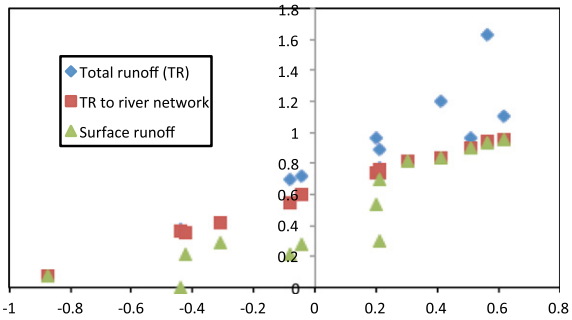

FIG. 8. In the ordinate, the TR and R (mm day^{-1}) generated by LSMs and the remaining TR flowing to the river network as functions of the optimal RE of simulated streamflows in the abscissa.

are different from 1. CLSM and CLSM-NASA are equal, or very close, to 0, due to the large values of surface runoff in the beginning of the wet season. For CLM, a large part of the total runoff is produced by surface runoff, and only ~30% of B is needed to simulate the observed river discharge. ARTS is not able to fully correct excessive R values, as the baseflow term only is fractioned with the f factor.

2) STREAMFLOW SIMULATIONS

Daily LSM-averaged streamflows produced by ARTS and standard deviations for THI and LAG experiments at five stations are presented in Figs. 9 and 10. LSM-averaged simulations for both experiments perform similarly at the selected locations, with NS values varying from 0.66 to 0.92. Timing is consistent with observations, with DI varying from −1 to 1 day. Missing or underestimated streamflow peak events in 2005 at Beterou and in 2005 and 2006 in Aval-Sani and Cote 238 derived from all realizations indicate issues in rainfall gauging over the western part of the basin. Although precipitation within the Donga River basin is highly monitored as reported in recent studies (e.g., Séguis et al. 2011), these results show that some precipitation events may have been missed.

Except for CLASS, ISBA, and SWAP, a significant overestimation of streamflows is noticed in the beginning of simulated wet seasons, as shown in Figs. 9 and 10. This is due to the fact that these models have low infiltration rates during those periods, generating more surface runoff than base flow. In this sense, the optimization algorithm tends to 1) minimize f as an attempt to reduce streamflows in that period and 2) increase τ_b as a way to delay the early discharge in rivers, resulting in a prolonged recession period. Other LSMs present a poor distribution of TR along the year, with low values during peaks. This counterbalances the

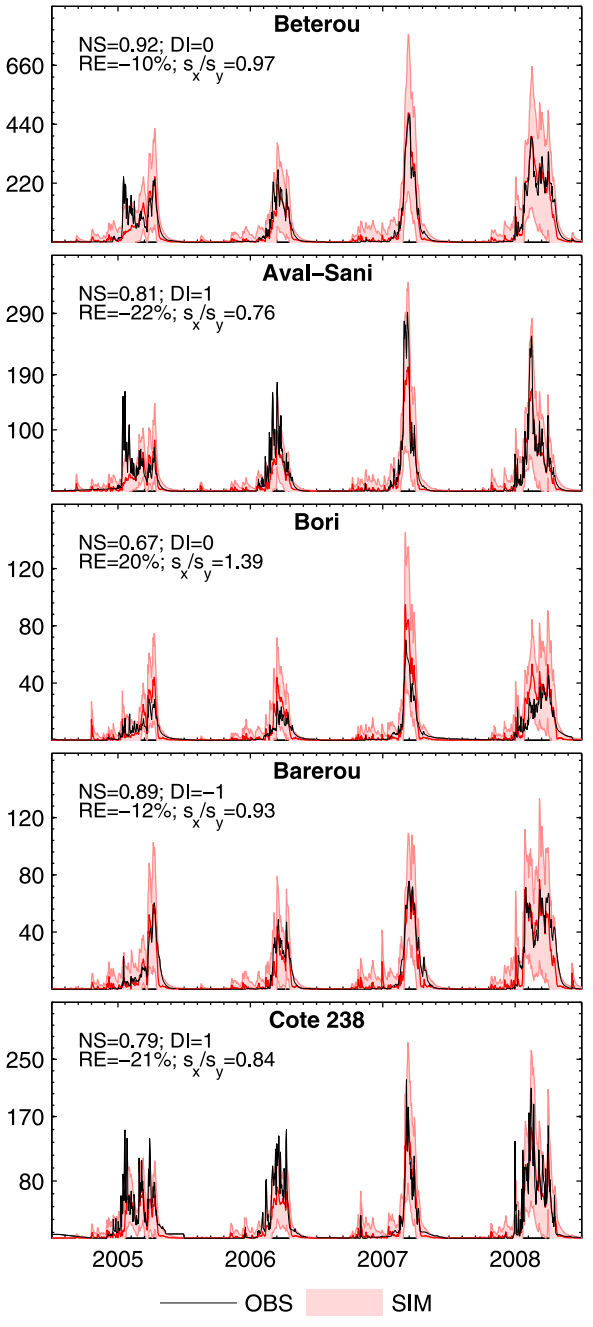

FIG. 9. Daily LSM-averaged streamflows ($m^3 s^{-1}$) and std dev for the THI-based precipitation experiment.

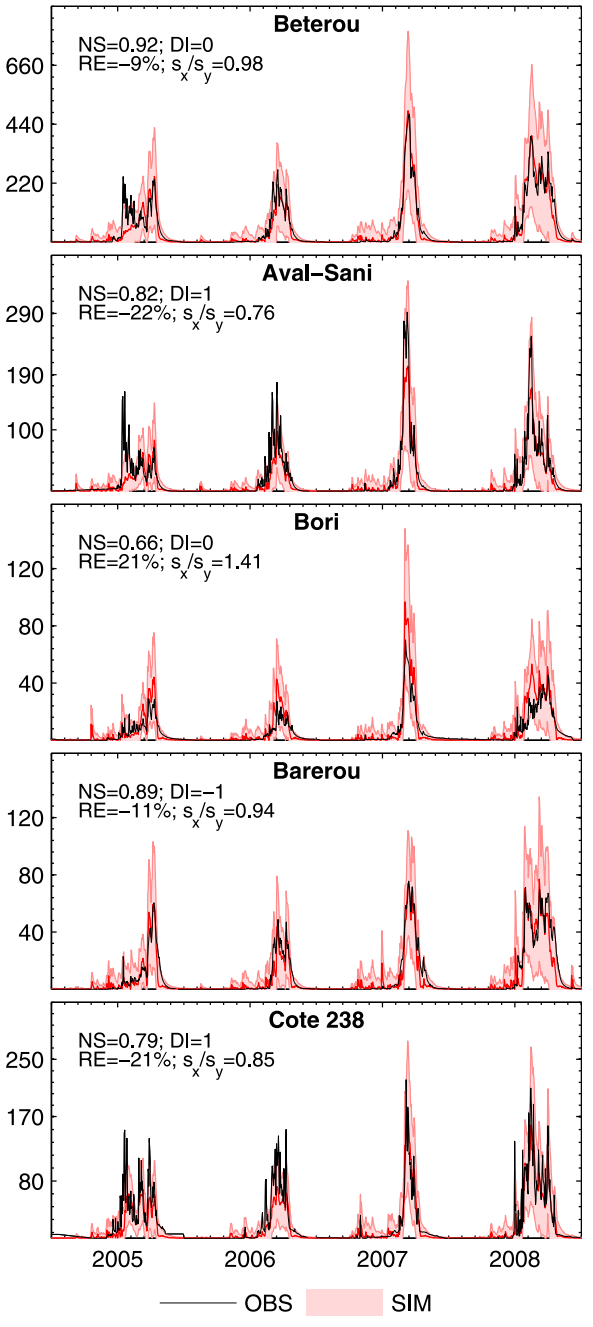

FIG. 10. As in Fig. 9, but for the LAG-based precipitation experiment.

effect of the overestimated TR in the beginning of the wet season on the optimization of f, described in (1). ISBA was capable of capturing the timing and amplitude of streamflow. Most THI realizations overestimate streamflow peaks, as a result of overestimated R rates. Exceptions are Noah, MATSIRO, and SETHYS, which underestimate the average streamflow when compared to observations.

Except for Bori, where LSMs generally overestimate streamflows by 20%–21%, simulated streamflows underestimate observations by 9%–22% across the basin. The standard deviation of the LSM ensemble is high, exceeding $340\,m^3 s^{-1}$ at Beterou in certain periods. Looking at daily seasonal cycles derived from the optimal result of each realization, as shown in Fig. 11, one can observe the general behavior of LSMs when forced

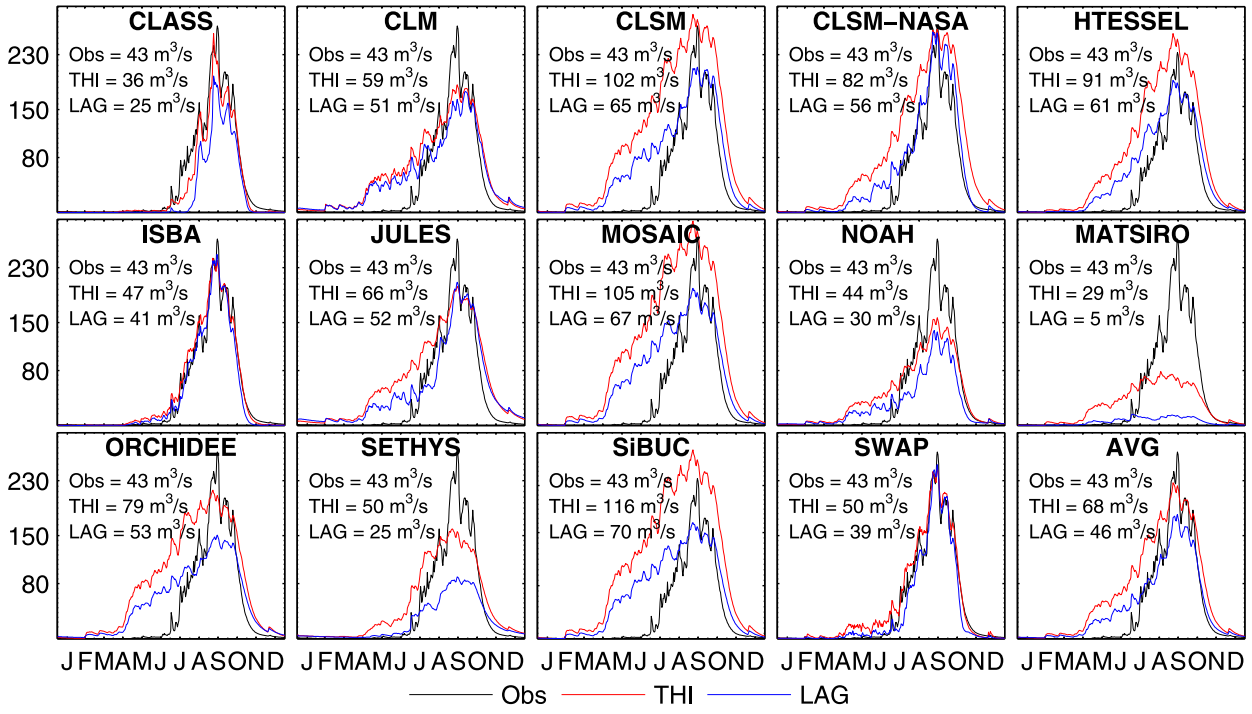

FIG. 11. Daily streamflow climatology at Beterou station ($m^3 s^{-1}$).

with both precipitation products. While some models show low sensitivity to changes in precipitation fields (e.g., CLASS, CLM, ISBA, and SWAP), others have a nonnegligible impact on simulated streamflows (e.g., CLSM, HTESSEL, MOSAIC, MATSIRO, SETHYS, and SiBUC). The latter LSMs provided average streamflows at least 50% higher when forced with THI.

Most models were able to represent peak amplitudes. However, except for CLASS and ISBA, all LSMs failed in representing the beginning of the wet season, showing early streamflows, up to 3–4 months before observations. This is related to the overestimated R generation as a result of reduced infiltration. A visual analysis of daily streamflow seasonal cycles confirms the superior performance of ISBA and SWAP. In particular, both experiments using ISBA show a very close fit with observations.

5. Summary

In the framework of phase 2 of the African Monsoon Multidisciplinary Analysis (AMMA) Land Surface Model Intercomparison Project (ALMIP2), the main goals of this paper are to assess how state-of-the-art LSM parameterizations reproduce the water budget and streamflow within a catchment controlled by a monsoon climate and the impact of precipitation datasets generated by two interpolation techniques [the Thiessen interpolation method (THI) and the combined kriging–Lagrangian methodology (LAG)] on the hydrological variables. Both interpolation techniques were applied to a dense rain gauge network available in the region. The goal was achieved by offline coupling 14 LSMs with the ALMIP2 River Routing Scheme (ARTS). These models were run for the upper Ouémé River basin (Benin, West Africa) forced with precipitation fields generated by THI and LAG, totaling 28 realizations. ARTS was run at the daily time step and 0.05° spatial resolution for the 2005–08 period. The MOCOM-UA algorithm was used to calibrate ARTS parameters for each LSM through the optimization of weighted averages of performance coefficients at five gauging stations within the basin.

It is shown that water budget simulations result in a wide range of evapotranspiration (ET), surface runoff R, and baseflow B rates. To evaluate the impacts of R and B ranges on streamflow simulation, three ARTS parameters were automatically calibrated for each realization. These parameters represent the surface runoff p_r and baseflow τ_b time delays and the fraction f of base flow converted into deep water infiltration (DWI). The automatic calibration of ARTS parameters resulted in optimal streamflows that were compared at five gauge stations within the basin. These results, along with parameter values, allowed us to evaluate LSM-based water budgets and to identify their strengths and weaknesses. All parameters show sensitivity to R and B values. Except for Noah, MATSIRO, and SETHYS, which

obtained optimal f values equal to ~1 (i.e., no water is diverged to the deep water aquifer), all LSMs showed an evident need for the representation of DWI. The use of such a robust solution was enough to obtain improved simulations of streamflow at gauges within the basin for LSMs overestimating base flow. On the other hand, no solution was proposed to resolve overestimated surface runoff. However, as stated in Getirana et al. (2014a), it is evident that this should be considered as a temporary solution until LSMs are improved to represent more detailed hydrological processes in the basin, notably more realistic groundwater representations.

According to the hypothesis suggested in Getirana et al. (2014a) in interpreting ISBA results, LSMs tend to underestimate ET in this region, as a consequence of misrepresented deep root zones, resulting in a limited access to water in deeper soil layers. In addition, we suggest that the seasonal dynamics of LAI also impacts the ET in terms of transpiration seasonality. The strong seasonality is confirmed in the experiments performed in this study, where ET climatology is relatively low due to low water availability for the vegetation during the dry season (which is also the potential evapotranspiration peak). Getirana et al. (2014a) also hypothesize that the underestimated ET is insufficient to explain the difference between simulated and observed streamflow, supporting the necessity to consider DWI as an additional physical process in some LSMs. Considering DWI in the modeling system is mostly motivated and supported by previous studies based on ground observation data where a significant fraction of the annual rainfall is turned into recharge rates (Kamagaté et al. 2007; Séguis et al. 2011). The inclusion of such a physical process in LSMs would create a new redistribution in the water balance where an additional reservoir should be taken into account (e.g., Vergnes et al. 2012). Overall, care must be taken when estimating water balance on such scales (herein), only considering the upper several meters of the soil when evaluating models using discharge since deeper long-term storage and exchanges are quite likely for basins, which can impact discharge. It is worthwhile to note that the analyses performed in this paper are not conclusive and that these are just hypotheses to be confirmed by detailed analyses and field experiments.

A comparison between precipitation products shows that the more complex interpolation process used in LAG increased the overall performance of models in simulating streamflows at all gauging stations used to evaluate streamflows within the basin. Even though that product provides a mean precipitation rate higher than THI, a nonnegligible impact on water budget variables is observed, which is probably due to differences in terms of the spatial and temporal distribution of rainfall within the basin. It is demonstrated that most LSMs have significant errors in the simulated TR, resulting in misrepresentation of streamflows during the beginning of wet seasons. This suggests that processes related to infiltration in such hydroclimatic and pedologic conditions should be better parameterized.

Acknowledgments. This work is supported by the African Monsoon Multidisciplinary Analysis (AMMA) project. Based on a French initiative, AMMA was built by an international scientific group and has been funded by a large number of agencies in France, the United Kingdom, the United States, and Africa. The ALMIP2 project is supported by AMMA, the French National Research Institute for Sustainable Development [Institut de recherche pour le développement (IRD)], Institut National des Sciences de l'Univers/Centre National de la Recherche Scientifique (INSU/CNRS) [France; Initiative Structurante Ecosphère continentale et côtière (EC2CO) and Les Enveloppes Fluides et l'Environnement (LEFE) programs]. Observed data were obtained in the framework of the AMMA-CATCH Observatory (http://www.amma-catch.org) and with the contribution of the scientific and technical teams from IRD and Direction Générale de l'Eau in Benin. Acknowledgements are due to Arnaud Zannou and Martial Dossou for providing streamflow dataset, and to Cedric H. David and an anonymous reviewer for their valuable comments.

APPENDIX

The ALMIP2 Working Group

Here is a list of the ALMIP2 working group members: S. Ait-Mesbah and J. Polcher (LMD, Paris, France); M. Anderson (USDA, Beltsville, MD); G. Balsamo, S. Boussetta, E. Dutra, F. Pappenberger, and C. Hain (ECMWF, Reading, United Kingdom); A. Boone, F. Favot, F. Guichard, A. Kaptue, and J.-L. Roujean (CNRM, Météo-France, Toulouse, France); B. Cappelaere, J. Demarty, C. Peugeot, L. Séguis, and C. Velluet (HydroSciences Montpellier, Montpellier, France); V. Chaffard, J. M. Cohard, T. Gascon, S. Galle, B. Hector, T. Lebel, T. Pellarin, A. Richard, G. Quantin, and T. Vischel [Laboratoire d'étude des Transferts en Hydrologie et Environnement (LTHE), Grenoble, France]; E. Chan and D. Verseghy [Climate Research Division, Environment and Climate Change Canada (ECCC), Toronto, Canada]; A. Ducharne and C. Magand [Milieux environnementaux, transferts et interactions dans les hydrosystèmes et les sols (METIS), Paris, France]; A. Getirana [NASA GSFC, Greenbelt,

MD, and Earth System Science Interdisciplinary Center (ESSIC), University of Maryland, College Park, College Park, MD]; M. Grippa, P. Hiernaux, L. Kergoat, E. Mougin, and C. Pierre (Geosciences Environnement Toulouse, Toulouse, France); Y. Gusev and O. Nasonova (Institute of Water Problems, Moscow, Russia); P. Harris [Center for Ecology and Hydrology (CEH), Wallingford, United Kingdom]; X. He (Institute of Industrial Science, University of Tokyo, Tokyo, Japan, and Dept. of Civil and Environmental Engineering, Princeton University, Princeton, NJ); K. Yorozu (Hydrology and Water Resources Research Laboratory, Kyoto University, Kyoto, Japan); S. Kotsuki and K. Tanaka [Rikagaku Kenkyusho (RIKEN) Advanced Institute for Computational Science, Kobe, Japan]; H. Kim and T. Oki (Institute of Industrial Science, University of Tokyo, Tokyo, Japan); S. Kumar (NASA GSFC, Greenbelt, MD); M.-H. Lo (Dept. of Atmospheric Sciences, National Taiwan University, Taipei, Taiwan); S. Mahanama (GMAO, NASA GSFC, Greenbelt, MD); F. Maignan and C. Ottlé [Laboratoire des Sciences du Climat et de l'Environnement (LSCE), Gif sur Yvette, France]; O. Mamadou (LTHE, Grenoble, France, and Institute of Mathematics and Physical Sciences, University of Porto-Novo, Porto-Novo, Bénin); and A. Shmakin, V. Sokratov, and D. Turkov (Institute of Geography, Russian Academy of Sciences, Moscow, Russia).

REFERENCES

Balsamo, G., F. Pappenberger, E. Dutra, P. Viterbo, and B. van den Hurk, 2011: A revised land hydrology in the ECMWF model: A step towards daily water flux prediction in a fully-closed water cycle. *Hydrol. Processes*, **25**, 1046–1054, doi:10.1002/hyp.7808.

Boone, A., and Coauthors, 2004: The Rhône-Aggregation Land Surface Scheme intercomparison project: An overview. *J. Climate*, **17**, 187–208, doi:10.1175/1520-0442(2004)017<0187:TRLSSI>2.0.CO;2.

——, and Coauthors, 2009a: AMMA Land Surface Model Intercomparison Project Phase 2 (ALMIP-2). *GEWEX News*, Vol. 19, No. 4, International GEWEX Project Office, Silver Spring, MD, 9–10. [Available online at http://www.gewex.org/gewex-content/files_mf/1432208883Nov2009.pdf.]

——, and Coauthors, 2009b: The AMMA Land Surface Model Intercomparison Project. *Bull. Amer. Meteor. Soc.*, **90**, 1865–1880, doi:10.1175/2009BAMS2786.1.

Boyle, D. P., H. V. Gupta, and S. Sorooshian, 2000: Toward improved calibration of hydrologic models: Combining the strengths of manual and automatic methods. *Water Resour. Res.*, **36**, 3663–3674, doi:10.1029/2000WR900207.

Clark, D. B., and Coauthors, 2011: The Joint UK Land Environment Simulator (JULES), model description—Part 2: Carbon fluxes and vegetation dynamics. *Geosci. Model Dev.*, **4**, 701–722, doi:10.5194/gmd-4-701-2011.

Coudert, B., C. Ottle, and X. Briottet, 2008: Monitoring land surface processes with thermal infrared data: Calibration of SVAT parameters based on the optimization of diurnal surface temperature cycling features. *Remote Sens. Environ.*, **112**, 872–887, doi:10.1016/j.rse.2007.06.024.

Cunge, J. A., 1969: On the subject of a flood propagation computation method (Muskingum method). *J. Hydraul. Res.*, **7**, 205–230, doi:10.1080/00221686909500264.

David, C. H., Z.-L. Yang, and S. Hong, 2013: Regional-scale river flow modeling using off-the-shelf runoff products, thousands of mapped rivers and hundreds of stream flow gauges. *Environ. Model. Software*, **42**, 116–132, doi:10.1016/j.envsoft.2012.12.011.

Decharme, B., C. Ottlé, S. Saux-Picart, N. Boulain, B. Cappelaere, D. Ramier, and M. Zribi, 2009: A new land surface hydrology within the Noah-WRF land–atmosphere mesoscale model applied to semiarid environment: Evaluation over the Dantiandou Kori (Niger). *Adv. Meteor.*, **2009**, 1–13, doi:10.1155/2009/731874.

Dirmeyer, P. A., A. Dolman, and N. Sato, 1999: The pilot phase of the Global Soil Wetness Project. *Bull. Amer. Meteor. Soc.*, **80**, 851–878, doi:10.1175/1520-0477(1999)080<0851:TPPOTG>2.0.CO;2.

——, X. Gao, M. Zhao, Z. Guo, T. Oki, and N. Hanasaki, 2006: GSWP-2: Multimodel analysis and implications for our perception of the land surface. *Bull. Amer. Meteor. Soc.*, **87**, 1381–1397, doi:10.1175/BAMS-87-10-1381.

Ducharne, A., R. D. Koster, M. J. Suarez, M. Stieglitz, and P. Kumar, 2000: A catchment-based approach to modeling land surface processes in a general circulation model: 2. Parameter estimation and model demonstration. *J. Geophys. Res.*, **105**, 24 823–24 838, doi:10.1029/2000JD900328.

Farr, T. G., and Coauthors, 2007: The Shuttle Radar Topography Mission. *Rev. Geophys.*, **45**, RG2004, doi:10.1029/2005RG000183.

Gaiser, T., and Coauthors, 2008: Development of a regional model for integrated management of water resources at the basin scale. *Phys. Chem. Earth*, **33**, 175–182, doi:10.1016/j.pce.2007.04.018.

Geiger, B., C. Meurey, D. Lajas, L. Franchistéguy, D. Carrer, and J.-L. Roujean, 2008: Near real-time provision of downwelling shortwave radiation estimates derived from satellite observations. *Meteor. Appl.*, **15**, 411–420, doi:10.1002/met.84.

Getirana, A. C. V., J. C. V. Espinoza, J. Ronchail, and O. C. Rotunno Filho, 2011: Assessment of different precipitation datasets and their impacts on the water balance of the Negro River basin. *J. Hydrol.*, **404**, 304–322, doi:10.1016/j.jhydrol.2011.04.037.

——, A. Boone, D. Yamazaki, B. Decharme, F. Papa, and N. Mognard, 2012: The Hydrological Modeling and Analysis Platform (HyMAP): Evaluation in the Amazon basin. *J. Hydrometeor.*, **13**, 1641–1665, doi:10.1175/JHM-D-12-021.1.

——, ——, ——, and N. Mognard, 2013: Automatic parameterization of a flow routing scheme driven by radar altimetry data: Evaluation in the Amazon basin. *Water Resour. Res.*, **49**, 614–629, doi:10.1002/wrcr.20077.

——, ——, and C. Peugeot, 2014a: Evaluating LSM-based water budgets over a West African basin assisted with a river routing scheme. *J. Hydrometeor.*, **15**, 2331–2346, doi:10.1175/JHM-D-14-0012.1.

——, and Coauthors, 2014b: Water balance in the Amazon basin from a land surface model ensemble. *J. Hydrometeor.*, **15**, 2586–2614, doi:10.1175/JHM-D-14-0068.1.

Giertz, S., B. Diekkrueger, and G. Steup, 2006: Physically-based modelling of hydrological processes in a tropical headwater

catchment (West Africa)—Process representation and multicriteria validation. *Hydrol. Earth Syst. Sci.*, **10**, 829–847, doi:10.5194/hess-10-829-2006.

Gusev, Y. M., and O. N. Nasonova, 1998: The land surface parameterization scheme SWAP: Description and partial validation. *Global Planet. Change*, **19**, 63–86, doi:10.1016/S0921-8181(98)00042-3.

Henderson-Sellers, A., A. J. Pitman, P. K. Love, P. Irannejad, and T. Chen, 1995: The Project for Intercomparison of Land-Surface Parameterization Schemes (PILPS): Phases 2 and 3. *Bull. Amer. Meteor. Soc.*, **76**, 489–503, doi:10.1175/1520-0477(1995)076<0489:TPFIOL>2.0.CO;2.

Kamagaté, B., L. Seguis, G. Favreau, J.-L. Seidel, M. Descloitres, and P. Affaton, 2007: Processus et bilan des flux hydriques d'un bassin versant de milieu tropical de socle au Benin (Donga, haut Ouémé). *C. R. Geosci.*, **339**, 418–429, doi:10.1016/j.crte.2007.04.003.

Kaptué Tchuenté, A. T., J.-L. Roujean, and S. M. De Jong, 2011: Comparison and relative quality assessment of the GLC2000, GLOBCOVER, MODIS and ECOCLIMAP land cover data sets at the African continental scale. *Int. J. Appl. Earth Obs. Geoinf.*, **13**, 207–219, doi:10.1016/j.jag.2010.11.005.

Kirpich, Z. P., 1940: Time of concentration of small agricultural watersheds. *Civ. Eng.*, **10** (6), 362.

Koster, R. D., and M. J. Suarez, 1992: Modeling the land surface boundary in climate models as a composite of independent vegetation stands. *J. Geophys. Res.*, **97**, 2697–2715, doi:10.1029/91JD01696.

——, ——, A. Ducharne, M. Stieglitz, and P. Kumar, 2000: A catchment-based approach to modeling land surface processes in a general circulation model: 1. Model structure. *J. Geophys. Res.*, **105**, 24 809–24 822, doi:10.1029/2000JD900327.

Krinner, G., and Coauthors, 2005: A dynamic global vegetation model for studies of the coupled atmosphere–biosphere system. *Global Biogeochem. Cycles*, **19**, 1–33, doi:10.1029/2003GB002199.

Lawrence, D. M., and Coauthors, 2011: Parameterization improvements and functional and structural advances in version 4 of the Community Land Model. *J. Adv. Model. Earth Syst.*, **3**, M03001, doi:10.1029/2011MS00045.

Lebel, T., and Coauthors, 2009: AMMA-CATCH studies in the Sahelian region of West Africa: An overview. *J. Hydrol.*, **375**, 3–13, doi:10.1016/j.jhydrol.2009.03.020.

Le Lay, M., G.-M. Saulnier, S. Galle, L. Seguis, M. Metadier, and C. Peugeot, 2008: Model representation of the Sudanian hydrological processes: Application on the Donga catchment (Benin). *J. Hydrol.*, **363**, 32–41, doi:10.1016/j.jhydrol.2008.09.006.

Li, H., L. R. Leung, A. Getirana, M. Huang, H. Wu, Y. Xu, J. Guo, and N. Voisin, 2015: Evaluating global streamflow simulations by a physically-based routing model coupled with the Community Land Model. *J. Hydrometeor.*, **16**, 948–971, doi:10.1175/JHM-D-14-0079.1.

Lohmann, D., and Coauthors, 1998: The Project for Intercomparison of Land-surface Parameterization Schemes (PILPS) phase 2(c) Red–Arkansas River basin experiment: 3. Spatial and temporal analysis of water fluxes. *Global Planet. Change*, **19**, 161–179, doi:10.1016/S0921-8181(98)00046-0.

Mamadou, O., J. M. Cohard, S. Galle, C. N. Awanou, A. Diedhiou, B. Kounouhewa, and C. Peugeot, 2014: Energy fluxes and surface characteristics over a cultivated area in Benin: Daily and seasonal dynamics. *Hydrol. Earth Syst. Sci.*, **18**, 893–914, doi:10.5194/hess-18-893-2014.

Noilhan, J., and J.-F. Mahfouf, 1996: The ISBA land surface parameterisation scheme. *Global Planet. Change*, **13**, 145–159, doi:10.1016/0921-8181(95)00043-7.

Pareto, V., 1971: *Manual of Political Economy*. A. M. Kelley, 504 pp.

Peugeot, C., and Coauthors, 2011: Mesoscale water cycle within the West African Monsoon. *Atmos. Sci. Lett.*, **12**, 45–50, doi:10.1002/asl.309.

Ponce, V. M., 1989: *Engineering Hydrology: Principles and Practices*. Prentice-Hall, 627 pp.

Séguis, L., and Coauthors, 2011: Origins of streamflow in a crystalline basement catchment in a sub-humid Sudanian zone: The Donga basin (Benin, West Africa): Inter-annual variability of water budget. *J. Hydrol.*, **402**, 1–13, doi:10.1016/j.jhydrol.2011.01.054.

Takata, K., S. Emori, and T. Watanabe, 2003: Development of the minimal advanced treatments of surface interaction and runoff. *Global Planet. Change*, **38**, 209–222, doi:10.1016/S0921-8181(03)00030-4.

Tanaka, K., and S. Ikebuchi, 1994: Simple Biosphere Model including Urban Canopy (SiBUC) for regional or basin-scale land surface processes. *Proc. Int. Symp. on GEWEX Asian Monsoon Experiment*, Beijing, China, Peking University, 59–62.

Trigo, I. F., and Coauthors, 2011: The Satellite Application Facility on Land Surface Analysis. *Int. J. Remote Sens.*, **32**, 2725, doi:10.1080/01431161003743199.

van den Hurk, B., and P. Viterbo, 2003: The Torne-Kalix PILPS 2(e) experiment as a test bed for modifications to the ECMWF land surface scheme. *Global Planet. Change*, **38**, 165–173, doi:10.1016/S0921-8181(03)00027-4.

——, M. Best, P. Dirmeyer, A. Pitman, J. Polcher, and J. Santanello, 2011: Acceleration of land surface model development over a decade of GLASS. *Bull. Amer. Meteor. Soc.*, **92**, 1593–1600, doi:10.1175/BAMS-D-11-00007.1.

Varado, N., I. Braud, S. Galle, M. Le Lay, L. Séguis, B. Kamagaté, and C. Depraetere, 2006: Multi-criteria assessment of the Representative Elementary Watershed approach on the Donga catchment (Benin) using a downward approach of model complexity. *Hydrol. Earth Syst. Sci.*, **10**, 427–442, doi:10.5194/hess-10-427-2006.

Vergnes, J.-P., B. Decharme, R. Alkama, E. Martin, F. Habets, and H. Douville, 2012: A simple groundwater scheme for hydrological and climate applications: Description and offline evaluation over France. *J. Hydrometeor.*, **13**, 1149–1171, doi:10.1175/JHM-D-11-0149.1.

Verseghy, D. L., 1991: Class—A Canadian land surface scheme for GCMS. I. Soil model. *Int. J. Climatol.*, **11**, 111–133, doi:10.1002/joc.3370110202.

Vischel, T., T. Lebel, S. Massuel, and B. Cappelaere, 2009: Conditional simulation schemes of rain fields and their application to rainfall–runoff modeling studies in the Sahel. *J. Hydrol.*, **375**, 273–286, doi:10.1016/j.jhydrol.2009.02.028.

Wood, E. F., and Coauthors, 1998: The Project for Intercomparison of Land-Surface Parameterization Schemes (PILPS) Phase-2c Red–Arkansas River basin experiment: 1. Experiment description and summary intercomparisons. *Global Planet. Change*, **19**, 115–139, doi:10.1016/S0921-8181(98)00044-7.

Yapo, P. O., H. V. Gupta, and S. Sorooshian, 1997: A multiobjective global optimization algorithm with application to

calibration of hydrologic models. HWR Tech. Rep. 97-050, The University of Arizona, 216 pp. [Available online at http://hdl.handle.net/10150/290649.]

——, ——, and ——, 1998: Multi-objective global optimization for hydrologic models. *J. Hydrol.*, **204**, 83–97, doi:10.1016/S0022-1694(97)00107-8.

Yilmaz, K. K., T. S. Hogue, K.-L. Hsu, S. Sorooshian, H. V. Gupta, and T. Wagener, 2005: Intercomparison of rain gauge, radar, and satellite-based precipitation estimates with emphasis on hydrologic forecasting. *J. Hydrometeor.*, **6**, 497–517, doi:10.1175/JHM431.1.

Zubieta, R., A. Getirana, J. C. Espinoza, W. Lavado, and M. Saavedra, 2015: Impacts of satellite-based precipitation datasets on the rainfall–runoff modeling of the Western Amazon basin (Peru and Ecuador). *J. Hydrol.*, **528**, 599–612, doi:10.1016/j.jhydrol.2015.06.064.